Exploiting Performance of Ambient Backscatter Systems in Presence of Hardware Impairment

Minh-Sang VAN NGUYEN [1] (iD), *Huu-Phuc DANG* [2] (iD)

[1]Department of Electronics and Telecommunications, Faculty of Electronics Technology,
Industrial University of Ho Chi Minh City (IUH), 12 Nguyen Van Bao, 700000 Ho Chi Minh City, Vietnam
[2]Electrical - Electronics Department, School of Engineering and Technology, Tra Vinh University,
126 Nguyen Thien Thanh, 87000 Tra Vinh, Vietnam

nguyenvanminhsang@iuh.edu.vn, danghuuphuc@tvu.edu.vn

Abstract. *In the context of ambient Backscatter systems, Backscatter devices (tags and readers) transmit data by employing existing Radio Frequency (RF) signals. Most prior works consider perfect hardware impairment and apply the Orthogonal Multiple Access (OMA) technique, but this paper investigates the case of Outage Probability (OP) reduction situation when the hardware is imperfect, especially when the Non-Orthogonal Multiple Access (NOMA) technology is applied. Consequently, we design a downlink of transmission from base station to destination to highlight different performances among users. Furthermore, to indicate the impact of levels of hardware impairment, we develop the closed-form expressions of OP for different kinds of users. Finally, extensive simulation results validate the analysis and illustrate the effectiveness of the proposed system.*

Keywords

Ambient Backscatter, hardware impairment, outage probability.

1. Introduction

To implement a unique symbiotic radio approach for the Internet of Things (IoT) to serve low-energy users, the Backscatter technique has been proposed as an emerging technique [1], [2], [3], [4], [5] and [6]. Under Backscatter Communication (BackCom) scenarios, the surrounding RF signals, such as cellular base stations, ambient TeleVision (TV) towers, and Wi-Fi access points, enable the Backscatter Device (BD) to convey information from them via throughput modulating and reflecting such received signals. To overcome the interference existing in the Backscatter receivers, one can deploy a cooperative ambient Backscatter system since both the primary system and the Backscatter that provides the RF carrier or the RF signals.

In recent times, many studies have proposed to use ambient Backscatter as a collaborative communication device in the IoT and cellular networks [7], [8], [9] and [10]. In particular, the authors in [7] presented the error performance of BackCom in the existence of ambient interference, in which a relay is the BD and the performance comparison is conducted by examining both Decode-and-Forward (DF) and Amplify-and-Forward (AF) based Backscatter relaying schemes. It is similar to [7], the work in [8] has also investigated the outage performance of the cooperative relaying system with the Backscatter application. By analyzing three different cases of the reflection coefficient, the authors have found the optimal reflection coefficients. The resource and power allocation problem of the collaborative ambient Backscatter system is addressed in [9]. Regarding the energy harvesting application in the ambient Backscatter system, the authors of [10] designed a Wireless Power Transfer (WPT) technique with the low-power BackCom to sustain battery-less wireless networks. In this paper, they deployed a Power Beacon Station (PBS) for a BackCom network wirelessly powered system. Reference [11] designed a proper waveform since the waveform was transmitted by a harvested energy-based reader. The authors in [12] explored dense BackCom systems by employing a dedicated energy source powered by Power

Beacons (PBs) into a BackCom system to provide signals for backscattering. They derived the formulas for the OP. It is noted that transmission capacity metric can be achieved using stochastic geometry. By jointly optimizing the relay strategy and the PB's beamforming for a PB-based BackCom network, the optimal system capacity can be achieved in [11]. By considering the value of the PB's transmit power, the time and the reflection coefficient in the PB can be evaluated, the authors in [13] studied the energy efficiency maximization for the wireless powered BackCom system.

A wide range of applications is considered for AmBackCom systems [14], [15], [16], [17], [18], [19] and [20]. More specifically, the authors in [14] designed the Plora as an ambient BD that application for batteryless IoT devices, the authors in [15] and [16] studied an AmBackCom system using the Maximum Likelihood (ML) detection where differential modulation is adopted in the tag. Further, the authors in [17] considered the Bit Error Rate (BER) using an ML detector. The work in [18] developed a time allocation factor to achieve the best throughput. The authors in [19] studied Backscatter cognitive radio networks by examining the throughput maximization for the secondary system. In [20] the authors studied the secondary system by considering different energy consumption models and the formula of ergodic capacity is computed. They considered joint optimization of the transmit power of the primary signal and the reflection coefficient of the secondary ambient Backscatter.

The authors in [21] investigated Multiple-Input Multiple-Output (MIMO) underlay spectrum-sharing systems by considering the performance of spatial modulation in three practical deleterious effects including outdated Channel State Information (CSI), transceiver Hardware Impairments (HIs) and imperfect CSI. By considering the joint impact of transceiver HIs and channel estimation errors, the authors in [22] studied the performance of a Cognitive DF Multi-Relay Network (CDFMRN) with a direct link. [23] examined massive MIMO-based distributed detection by considering transceiver HIs at both a massive-antenna Fusion Center (FC) and multiple single-antenna sensors. There is a wonderful association of Backscatter with NOMA that is shown in [24], [25] and [26]. Specifically, the authors in [24] have proposed a NOMA-Backscatter system and its application in a symbiotic system of cellular and IoT networks. As an updated version of [24], the authors in [25] have studied the application of NOMA-Backscatter system to cellular networks, the research results have shown that the system achieves outstanding performance when increasing the number of antennas at the Base Station (BS). The work in [26] proposed the combination of Reconfigurable Intelligent Surface (RIS) with NOMA as a good solution to help reduce power consumption and hardware cost

as well as increase the network performance. In addition, the effects of hardware impairment on Multi-relay networks and NOMA Full-Duplex networks were examined in detail in [27] and [28], respectively.

From the above analysis, it has been shown that the ambient Backscatter system is considered a promising technology that is receiving a lot of attention and research. However, there are very few works that considered the Backscatter system in the existence of HIs [29]. We are motivated by the above analysis and novel results in [24] and [29], this paper considers degraded system performance metric, i.e. OP, to evaluate the performance of users in the primary and Backscatter networks. The main contributions and novelty of our work are shown as follows:

- We propose a novel Symbiotic communication model using Backscatter combine with the NOMA scheme, namely NOMA-Backscatter. Especially Backscatter's imperfect hardware is also considered.

- From the proposed model, we derive the closed-forms of OP as a function of transmitting Signal-to-Noise Ratio (SNR). Furthermore, the key parameters affecting the system performance are also carefully analyzed and evaluated.

- Next, the Monte Carlo simulations present the outage performance to validate our analysis. Our research results have shown that the outage performance of the NOMA-Backscatter system can be significantly enhanced compared to the conventional OMA-Backscatter scheme.

2. System Model

A cooperative ambient NOMA-Backscatter system is examined as Fig. 1. In this model, a Primary Transmitter (PT) intends to send a signal to a primary receiver (D_P) and IoT receiver (D_I) in the context of the NOMA scheme. Precisely, the PT will broadcast the superposition signal $x(k) = \sqrt{\alpha_1}x_1(k) + \sqrt{\alpha_2}x_2(k)$ to other devices in the networks, where $x_i(k)$ and α_i, $(i = 1, 2)$ denotes the information symbols and the power allocation coefficients of D_I and D_P, respectively, such that $\alpha_1 + \alpha_2 = 1$ and $\alpha_1 < \alpha_2$. In addition, to enhance the information transmission from PT to D_I and from PT to D_P, a Backscatter device, namely BD, has been implemented to support signal forwarding in the network system. In this context, we will analyze two possible scenarios: the BD only serves D_I corresponding to Scheme 1 and the BD serves both D_I and D_P that corresponding to Scheme 2.
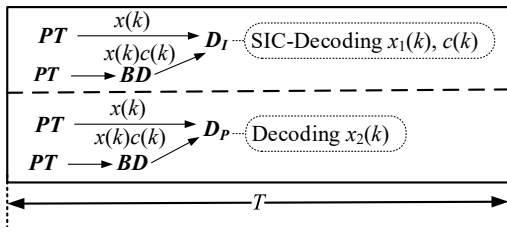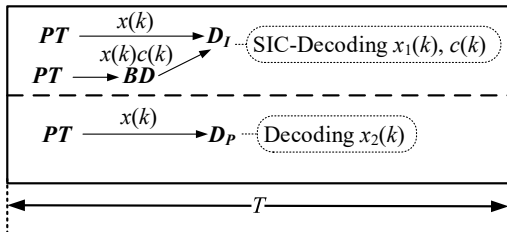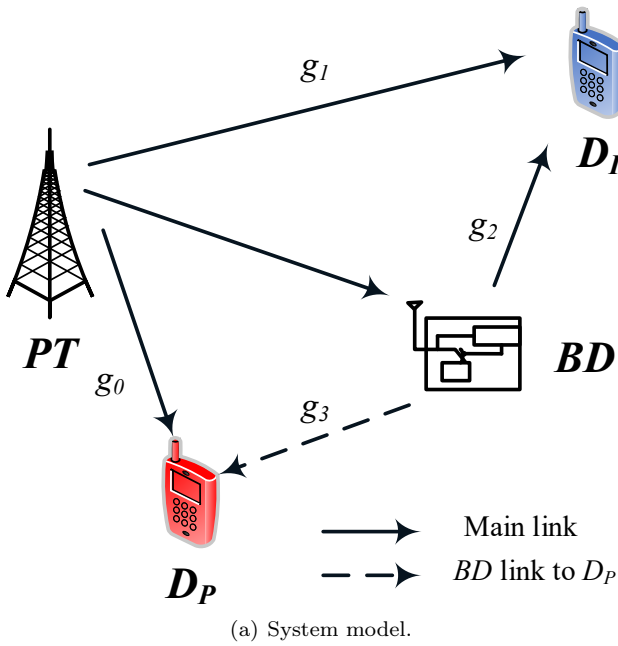
(a) System model.

(b) Timing diagram with Scheme 1.

(c) Timing diagram with Scheme 2.

Fig. 1: The ambient system.

Tab. 1: Mathematical notations used in this article.

Symbol	Description
Pr (.)	Probability of an event
$CN(m, n)$	Complex Gaussian distribution with mean m and variance n
E [.]	Expectation operator
$x_1(k)$	The k-th symbol to be transmitted by PT to D_I
$x_1(k)$	The k-th symbol to be transmitted by PT to D_P
α_1	Power allocation parameters of D_I
α_2	Power allocation parameters of D_P
$c(k)$	The k-th symbol to be transmitted by BD
P	The transmit power at PT
$\sigma_I(k)$	The Additive White Gaussian Noise (AWGN) with $CN(0, N_0)$
$\sigma_P(k)$	The normalized AWGN at D_P with $CN(0, N_0)$
τ_I	The threshold SNR at D_I [8]
τ_{BD}	The threshold SNR at BD
τ_P	The threshold SNR at D_P
κ_{PT}	The transmitted and received aggregate level of impairments at PT [27] and [28]
κ_I	The transmitted and received aggregate level of impairments at D_I
κ_R	The transmitted and received aggregate level of impairments at D_R
ε	The normalized reflection coefficient of BD with $0 \le \varepsilon \le 1$ [8] and [9]
β	The backscatter efficiency with $\beta \le 1$ [8] and [9]
g_0	The Rayleigh fading channel responses from the $PT \to D_P$ with channel gains following as $g_0 \sim CN(0, \eta_0)$
g_1	The Rayleigh fading channel responses from the $PT \to D_I$ with channel gains following as $g_1 \sim CN(0, \eta_1)$
g_2	The Rayleigh fading channel responses from the $PT \to BD \to D_I$ with channel gains following as $g_2 \sim CN(0, \eta_2)$
g_3	The Rayleigh fading channel responses from the $PT \to BD \to D_P$ with channel gains following as $g_3 \sim CN(0, \eta_3)$

2.1. Scheme 1: The BD Only Serves D_I

In this scenario, We assume that only D_I is accessible by the BD, a passive BD conveys its own signal by riding on the RF signal from PT. The received signal at the D_I can be written as ([8] and [27]):

$$y_I = g_1 (x(k) + \mu_{PT}) + \mu_I + \\ + \sqrt{\varepsilon \beta P} g_2 c(k) x(k) + \sigma_I(k), \qquad (1)$$

where we can see the main parameters that are described in Tab. 1. In addition, $x_i(k)$, $(i = 1, 2)$ and $c(k)$ are distributed as independent and identically distributed (i.i.d.) zero-mean circularly symmetric complex. It is noted that symbols have their normalized

variance of $\mathrm{E}\left[|x_i(k)|^2\right] = 1$ and $\mathrm{E}\left[|c(k)|^2\right] = 1$. μ_{PT} and μ_I are the distortion noise with zero mean and variance $\kappa_{PT}^2 P$ and $\kappa_I^2 P |g_1|^2$, respectively.

As in [9], by utilizing Successive Interference Cancellation (SIC), user D_I recovers $c(k)$. To decode the backscatter signal $c(k)$, the user D_I first decodes $x_2(k)$ by treating the signal $x_1(k)$ and $c(k)$ as interference, then decodes $x_1(k)$ and finally $c(k)$ with the SIC technique.

We continue to compute the Signal-to-Interference-plus-Noise Ratio (SINR) to decode $x_2(k)$, SINR is given by:

$$\gamma_{I,2} = \frac{\alpha_2 \rho |g_1|^2}{\alpha_1 \rho |g_1|^2 + (\kappa_{PT}^2 + \kappa_I^2) \rho |g_1|^2 + \varepsilon \beta \rho |g_2|^2 + 1}, \qquad (2)$$

where $\rho = \frac{P}{N_0}$.

Then, SNR is used to decode $x_1(k)$ and it is formulated by:

$$\gamma_I = \frac{\alpha_1 \rho |g_1|^2}{\left(\kappa_{PT}^2 + \kappa_I^2\right)\rho |g_1|^2 + \varepsilon\beta\rho|g_2|^2 + 1}. \qquad (3)$$

Finally, SNR is used to decode $c(k)$ and it is formulated by:

$$\gamma_{BD} = \frac{\varepsilon\beta\rho|g_2|^2}{\left(\kappa_{PT}^2 + \kappa_I^2\right)\rho|g_1|^2 + 1}. \qquad (4)$$

Next, the signal received at D_P can be computed by:

$$y_P = g_0\left(\sqrt{\alpha_1 P}x_1(k) + \sqrt{\alpha_2 P}x_2(k) + \mu_{PT}\right) + \\ + \mu_R + \sigma_P(k), \qquad (5)$$

where μ_R is the distortion noise with zero mean and variance $\kappa_R^2 P|g_0|^2$.

Therefore, the SNR to decode $x_2(k)$ at D_P is given as:

$$\gamma_P = \frac{\alpha_2\rho|g_0|^2}{\alpha_1\rho|g_0|^2 + \left(\kappa_{PT}^2 + \kappa_R^2\right)\rho|g_0|^2 + 1}. \qquad (6)$$

2.2. Scheme 2: The BD Serves Both D_I and D_P

In this part, we consider the assumption that the BD can transmit the signal to the D_P. Therefore, the received signal at the D_P can be expressed as:

$$y_{2,P} = g_0\left(x(k) + \mu_{PT}\right) + \mu_R + \\ + \sqrt{\varepsilon\beta P}g_3 c(k)x(k) + \sigma_P(k). \qquad (7)$$

Therefore, the SNR to decode $x_2(k)$ at D_P is given as:

$$\gamma_{2,PT} = \frac{\alpha_2\rho|g_0|^2}{\alpha_1\rho|g_0|^2 + \left(\kappa_{PT}^2 + \kappa_R^2\right)\rho|g_0|^2 + \varepsilon\beta\rho|g_3|^2 + 1}. \qquad (8)$$

3. Performance Analysis

In this section, the analytical expressions of the OP for D_I, BD and D_P are derived to reflect the performance of the considered system.

It is noted that all channels follow the Rayleigh distribution with the Cumulative Distribution Function (CDF) and the Probability Density Function (PDF) can be expressed by $F_{|g_u|^2}(x) = 1 - \exp\left(-\frac{x}{\eta_u}\right)$ and $f_{|g_u|^2}(x) = \frac{1}{\eta_u}\exp\left(-\frac{x}{\eta_u}\right)$, where $u \in \{0,1,2,3\}$.

3.1. OP of D_I

For D_I, the outage event will not occur when D_I can successfully decode signal $x_2(k)$ and $x_1(k)$ from PT.

Thus the OP of D_I can be expressed as [24]:

$$P_{\text{out}}^{(I)} = \Pr\left(\gamma_{I,2} < \tau_P, \gamma_I < \tau_I\right) = \\ = 1 - \underbrace{\Pr\left(\gamma_{I,2} \geq \tau_P, \gamma_I \geq \tau_I\right)}_{\Omega}. \qquad (9)$$

The complementary event Ω in the expression Eq. (9) can be rewritten as:

$$\Omega = \Pr\left(\begin{array}{c}\frac{\alpha_2\rho|g_1|^2}{\alpha_1\rho|g_1|^2+\kappa_1\rho|g_1|^2+\varepsilon\beta\rho|g_2|^2+1} \geq \tau_P, \\ \frac{\alpha_1\rho|g_1|^2}{\kappa_1\rho|g_1|^2+\varepsilon\beta\rho|g_2|^2+1} \geq \tau_I\end{array}\right) = \\ = \Pr\left(\begin{array}{c}|g_1|^2 \geq \frac{\left(\varepsilon\beta\rho|g_2|^2+1\right)}{\rho} \\ \max\left(\frac{\tau_P}{(\alpha_2-\tau_P\alpha_1-\tau_P\kappa_1)}, \frac{\tau_I}{(\alpha_1-\tau_I\kappa_1)}\right)\end{array}\right), \qquad (10)$$

in which $\kappa_1 = \kappa_{PT}^2 + \kappa_I^2$, we let $\theta = \max\left(\frac{\tau_P}{(\alpha_2-\tau_P\alpha_1-\tau_P\kappa_1)}, \frac{\tau_I}{(\alpha_1-\tau_I\kappa_1)}\right)$ and it is noted that strict constraint here is $\alpha_2 > \tau_P\alpha_1 + \tau_P\kappa_1, \alpha_1 > \tau_I\kappa_1$. Therefore, Ω can be given as:

$$\Omega = \Pr\left(|g_1|^2 \geq \frac{\left(\varepsilon\beta\rho|g_2|^2 + 1\right)\theta}{\rho}\right) = \\ = \int_0^\infty \left(1 - F_{|g_1|^2}\left(\frac{(\varepsilon\beta\rho x + 1)\theta}{\rho}\right)\right)f_{|g_2|^2}(x)\,dx. \qquad (11)$$

Base on CDF and PDF of $|g_1|^2$ and $|g_2|^2$, Ω can be given as:

$$\Omega = \int_0^\infty \exp\left(-\frac{(\varepsilon\beta\rho x + 1)\theta}{\rho\eta_1}\right)\frac{1}{\eta_2}\exp\left(-\frac{x}{\eta_2}\right)dx = \\ = \frac{1}{\eta_2}\exp\left(-\frac{\theta}{\rho\eta_1}\right)\int_0^\infty \exp\left(-\left(\frac{\theta\varepsilon\beta}{\eta_1} + \frac{1}{\eta_2}\right)x\right)dx = \\ = \frac{1}{\eta_2}\exp\left(-\frac{\theta}{\rho\eta_1}\right)\frac{1}{\frac{\theta\varepsilon\beta}{\eta_1} + \frac{1}{\eta_2}} = \\ = \frac{\eta_1}{\theta\varepsilon\beta\eta_2 + \eta_1}\exp\left(-\frac{\theta}{\rho\eta_1}\right). \qquad (12)$$

Continuing to perform some simple calculations, we can obtain $P_{\text{out}}^{(I)}$ as following proposition.

Proposition 1: For D_I, the OP of the Backscatter system can be expressed as:

$$P_{\text{out}}^{(I)} = 1 - \frac{\eta_1}{\theta\varepsilon\beta\eta_2 + \eta_1}\exp\left(-\frac{\theta}{\rho\eta_1}\right). \qquad (13)$$

3.2. OP of BD

If D_I fails to decode $x_i(k)$ or $c(k)$, the outage event for BD occurs, and thus the OP of BD can be expressed

as [24]:

$$P_{\text{out}}^{(BD)} = 1 - \Pr\left(\gamma_{I,2} \geq \tau_P, \gamma_I \geq \tau_I, \gamma_{BD} \geq \tau_{BD}\right) =$$
$$= 1 - \underbrace{\Pr\left(\gamma_{I,2} \geq \tau_P, \gamma_I \geq \tau_I\right)}_{\Theta_1}\underbrace{\Pr\left(\gamma_{BD} \geq \tau_{BD}\right)}_{\Theta_2}.$$

(14)

From Eq. (14), Θ_1 is calculated similarly to Eq. (12). Further, Θ_2 can be written as:

$$\Theta_2 = \Pr\left(\gamma_{BD} \geq \tau_{BD}\right) = \Pr\left(\frac{\varepsilon\beta\rho|g_2|^2}{\kappa_1\rho|g_1|^2 + 1} \geq \tau_{BD}\right) =$$
$$= \Pr\left(|g_2|^2 \geq \frac{\tau_{BD}\left(\kappa_1\rho|g_1|^2 + 1\right)}{\varepsilon\beta\rho}\right) =$$
$$= \int_0^\infty \left(1 - F_{|g_2|^2}\left(\frac{\tau_{BD}\left(\kappa_1\rho x + 1\right)}{\varepsilon\beta\rho}\right)\right)f_{|g_1|^2}(x)\,dx.$$

(15)

Base on CDF and PDF of $|g_1|^2$ and $|g_1|^2$, Θ_2 can be given as:

$$\Theta_2 = \frac{1}{\eta_1}\exp\left(-\frac{\tau_{BD}}{\varepsilon\beta\rho\eta_2}\right)\cdot$$
$$\cdot\int_0^\infty \exp\left(-\left(\frac{\tau_{BD}\kappa_1}{\varepsilon\beta\eta_2} + \frac{1}{\eta_1}\right)x\right)dx =$$
$$= \frac{1}{\eta_1}\exp\left(-\frac{\tau_{BD}}{\varepsilon\beta\rho\eta_2}\right)\frac{1}{\frac{\tau_{BD}\kappa_1}{\varepsilon\beta\eta_2} + \frac{1}{\eta_1}} =$$
$$= \frac{\varepsilon\beta\eta_2}{\tau_{BD}\kappa_1\eta_1 + \varepsilon\beta\eta_2}\exp\left(-\frac{\tau_{BD}}{\varepsilon\beta\rho\eta_2}\right).$$

(16)

From Eq. (12) and Eq. (16) into Eq. (14), the closed-form formula of the OP for user BD as *Proposition 2* below.

Proposition 2: The closed-form of OP for user BD is given by:

$$P_{\text{out}}^{(BD)} = 1 - \frac{\eta_1}{\theta\varepsilon\beta\eta_2 + \eta_1}\exp\left(-\frac{\theta}{\rho\eta_1}\right)\cdot$$
$$\cdot\frac{\varepsilon\beta\eta_2}{\tau_{BD}\kappa_1\eta_1 + \varepsilon\beta\eta_2}\exp\left(-\frac{\tau_{BD}}{\varepsilon\beta\rho\eta_2}\right) =$$
$$= 1 - \frac{\eta_1}{\theta\varepsilon\beta\eta_2 + \eta_1}\frac{\varepsilon\beta\eta_2}{\tau_{BD}\kappa_1\eta_1 + \varepsilon\beta\eta_2}\cdot$$
$$\cdot\exp\left(-\frac{\theta}{\rho\eta_1} - \frac{\tau_{BD}}{\varepsilon\beta\rho\eta_2}\right).$$

(17)

3.3.   OP of D_P in Scheme 1

The outage events of D_P occur when D_P cannot decode message $x_2(k)$ from PT successfully. The OP of D_P is

expressed as:

$$P_{\text{out}}^{(P)} = \Pr\left(\gamma_P < \tau_P\right) =$$
$$= 1 - \Pr\left(\frac{\alpha_2\rho|g_0|^2}{\alpha_1\rho|g_0|^2 + \left(\kappa_{PT}^2 + \kappa_R^2\right)\rho|g_0|^2 + 1} \geq \tau_P\right) =$$
$$= 1 - \Pr\left(|g_0|^2 \geq \frac{\tau_P}{\left(\alpha_2 - \tau_P\alpha_1 - \tau_P\kappa_2\right)\rho}\right) =$$
$$= 1 - \exp\left(-\frac{\tau_P}{\left(\alpha_2 - \tau_P\alpha_1 - \tau_P\kappa_2\right)\rho\eta_0}\right),$$

(18)

where $\kappa_2 = \kappa_{PT}^2 + \kappa_R^2$.

3.4.   OP of D_P in Scheme 2

The outage events of D_P, in this case, may occur when D_P cannot successfully decode message $x_2(k)$ from PT. Therefore, the OP of D_P is expressed as [24] in Eq. (19).

3.5.   Asymptotic OP

To have a better understanding of the outage behavior, we investigate the asymptotic of the OP by considering $\rho \to \infty$. Consequently, the asymptotic expression for OP at D_I, BD and D_P are respectively written by:

$$P_{\text{asym}}^{(I)} = 1 - \frac{\eta_1}{\theta\varepsilon\beta\eta_2 + \eta_1},$$

(20)

$$P_{\text{asym}}^{(BD)} = 1 - \frac{\eta_1}{\theta\varepsilon\beta\eta_2 + \eta_1}\frac{\varepsilon\beta\eta_2}{\tau_{BD}\kappa_1\eta_1 + \varepsilon\beta\eta_2},$$

(21)

$$P_{\text{asym}}^{(P)} = 0,$$

(22)

$$P_{\text{asym}}^{(2,PT)} = 1 - \frac{\left(\alpha_2 - \tau_P\alpha_1 - \tau_P\kappa_2\right)\eta_0}{\tau_P\varepsilon\beta\eta_3 + \left(\alpha_2 - \tau_P\alpha_1 - \tau_P\kappa_2\right)\eta_0}.$$

(23)

4.   Simulation Results

In this section, the correctness of the theoretical results is verified by Monte Carlo simulations. Unless other stated, the main simulated parameters values of the Monte Carlo simulation can see in Tab. 2.

In Fig. 2, we plot the outage performance of three users, D_I, D_P and BD for Scheme 1, which are versus transmit ρ at the PT. The curves in this figure are derived from the analytical results in Eq. (13), Eq. (17), Eq. (18), Eq. (20), and Eq. (21), respectively. Since the OP is a function of ρ, the higher ρ results in the lower OP, which is equivalent to a better outage performance. It should be noted that the user D_P does not reflect factor in this scheme while two users D_I and BD have the impact of ε. In addition, it can be seen from Fig. 2 that the higher the reflection coefficient, the worse outage performance of D_I and BD gets. This

$$P_{\text{out}}^{(2,PT)} = \Pr\left(\gamma_{2,PT} < \tau_P\right) = 1 - \Pr\left(\frac{\alpha_2\rho|g_0|^2}{\alpha_1\rho|g_0|^2 + \kappa_2\rho|g_0|^2 + \varepsilon\beta\rho|g_3|^2 + 1} \geq \tau_P\right) =$$

$$= 1 - \Pr\left(|g_0|^2 \geq \frac{\tau_P\left(\varepsilon\beta\rho|g_3|^2 + 1\right)}{(\alpha_2 - \tau_P\alpha_1 - \tau_P\kappa_2)\rho}\right) = 1 - \int_0^\infty \left(1 - F_{|g_0|^2}\left(\frac{\tau_P\left(\varepsilon\beta\rho x + 1\right)}{(\alpha_2 - \tau_P\alpha_1 - \tau_P\kappa_2)\rho}\right)\right) f_{|g_3|^2}(x)\, dx =$$

$$= 1 - \frac{1}{\eta_3}\exp\left(-\frac{\tau_P}{(\alpha_2 - \tau_P\alpha_1 - \tau_P\kappa_2)\rho\eta_0}\right) \int_0^\infty \exp\left(-\left(\frac{\tau_P\varepsilon\beta}{(\alpha_2 - \tau_P\alpha_1 - \tau_P\kappa_2)\eta_0} + \frac{1}{\eta_3}\right)x\right)dx =$$

$$= 1 - \frac{(\alpha_2 - \tau_P\alpha_1 - \tau_P\kappa_2)\eta_0}{\tau_P\varepsilon\beta\eta_3 + (\alpha_2 - \tau_P\alpha_1 - \tau_P\kappa_2)\eta_0}\exp\left(-\frac{\tau_P}{(\alpha_2 - \tau_P\alpha_1 - \tau_P\kappa_2)\rho\eta_0}\right).$$

$$(19)$$

Tab. 2: Main parameters for numerical results [8] and [28].

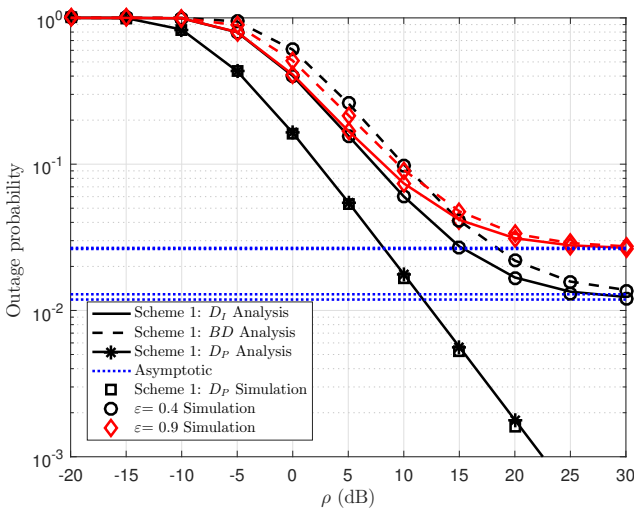| Parameter	Value
Power allocation parameters	$\alpha_1 = 0.4$, $\alpha_2 = 0.6$
The normalized reflection coefficient	$\varepsilon = 0.6$
The threshold SNR	$\tau_I = \tau_P = -10$ (dB), $\tau_{BD} = -20$ (dB)
Channel gains	$\eta_0 = 1$, $\eta_1 = 0.5$, $\eta_2 = \eta_3 = 0.1$
Hardware impairment levels	$\kappa = \kappa_{PT} = \kappa_I = \kappa_R = 0.05$

Fig. 2: Outage performance comparisons of the backscatter systems versus SNR as changing ε.

can be explained by increasing the reflection coefficient ε which causes the interference from Backscatter to increase and as a result, the system performance decreases. In this circumstance, $\varepsilon = 0.4$ is reported as the better case. At high ρ regime, OP performance of D_I and BD meets floor value while OP performance of D_P has significant improvement. Furthermore, The absolute match between the simulation curves and the analytical curves showed the correctness of our analysis and calculation above.

Figure 3 shows the comparison of D_P's outage performance in the presence and absence of BD link corresponds to Scheme 1 and Scheme 2. We can easily see
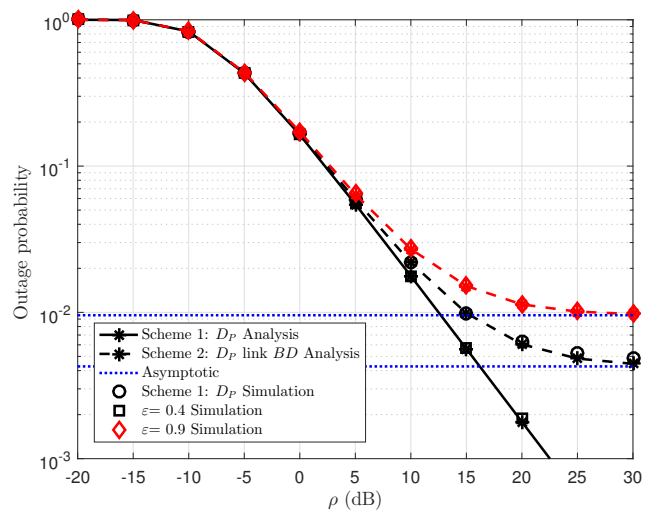

Fig. 3: Outage performance comparisons of D_P in Scheme 1 and Scheme 2 versus ρ.

from Fig. 3 that Scheme 1 has a far superior outage performance than Scheme 2 in the high SNR region. The key explanation for this is that the interference signal from the BD induces an outage performance decrease.
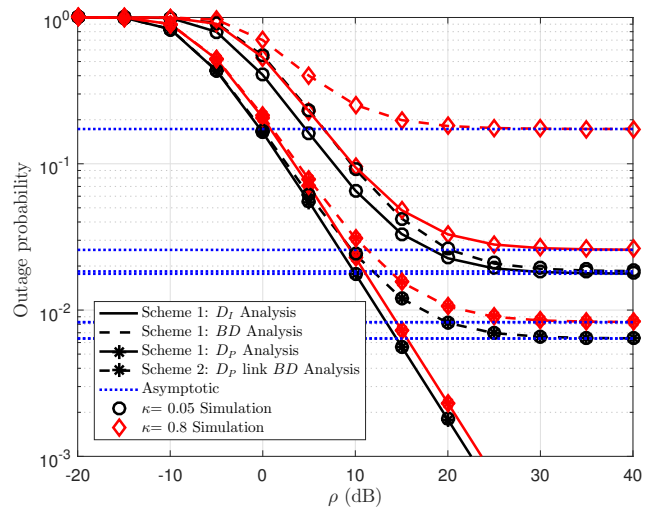

Fig. 4: Outage performance comparisons of the backscatter systems versus ρ as changing $\kappa = \kappa_{PT} = \kappa_I = \kappa_R$.

In Fig. 4, the impact of hardware impairment on OP performance can be reported. In particular, lower hardware impairment, $\kappa = \kappa_{PT} = \kappa_I = \kappa_R = 0.05$ leads to the better performance among two considered cases.

By assigning different power levels to each signal for users D_I, D_P, we can achieve differences among the performance of two users, shown in Fig. 5. It can be explained that α_1, α_2 lead to different power to processing signals for two users, which is confirmed by considering the expression Eq. (1). Besides, increasing the α_1 means that α_2 is reduced as well, and therefore, when the value of α_1 is enhanced, the outage performance of D_I will obviously increase while the outage performance of the D_P will be decreased.
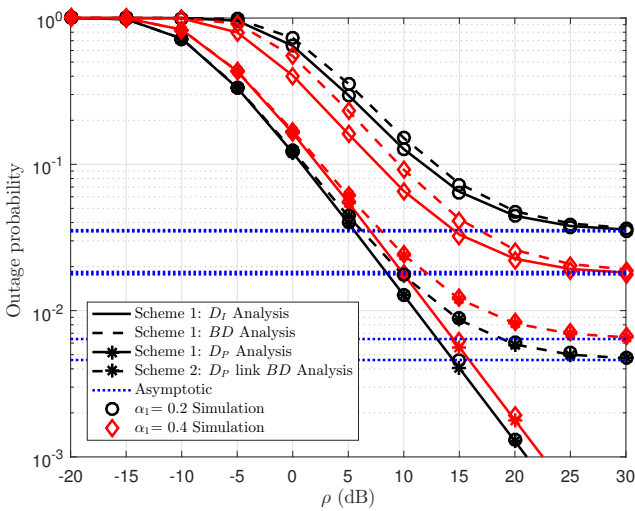

Fig. 5: Outage performance comparisons of the backscatter systems versus ρ as changing α_1.
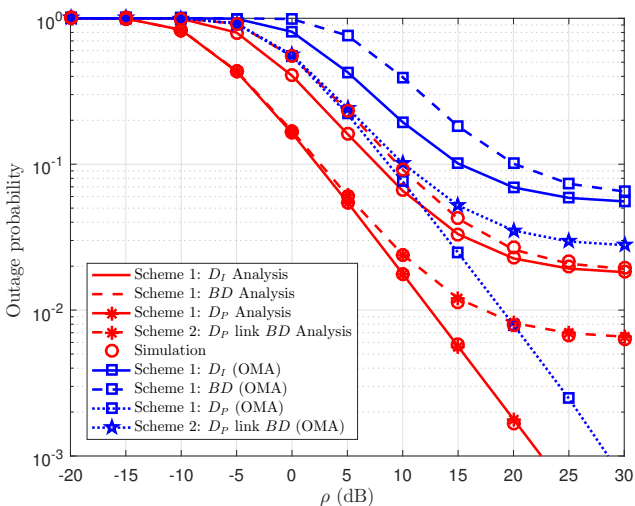

Fig. 6: Outage performance comparisons of the Backscatter systems and OMA versus ρ.

In Fig. 6, we compared the outage performance of the proposed NOMA-Backscatter with the OMA scheme,

where PT would transmit $x_1(k)$, $x_2(k)$, and sine wave signals for D_I, D_P, and BD in three orthogonal time slots, respectively, to verify the potential performance improvement of the proposed system model. It can be clearly seen from Fig. 6 that the outage performance of NOMA-Backscatter outperforms the OMA scheme.

5.   Conclusion

This paper has studied the performance of three kinds of users in the ambient BackComs underlying cellular system in the context of hardware impairment and the information transmission is based on the NOMA principle. In particular, we derived the outage probabilities for destinations in the primary networks and users in downlink transmissions of the Backscatter networks. We indicated the impact of various main parameters on such outage performance. Our results confirmed that the outage performance of the NOMA-Backscatter system can be significantly improved by selecting a reflecting and Backscatter ratio and our proposed schemes can achieve lower outage capacities at high SNR region. It also shows that the use of the outage performance is affected by levels of HIs. We provided detailed guidelines for design Backscatter in poor condition as under a situation of imperfect hardware.

Author Contributions

H.-P.D. developed the theoretical formalism, performed the analytic calculations, and supervised the project. M.-S.V.N. performed the numerical simulations. Both H.-P.D. and M.-S.V.N. authors contributed to the final version of the manuscript.

References

[1] HUYNH, N. V., D. T. HOANG, X. LU, D. NIYATO, P. WANG and D. I. KIM. Ambient Backscatter Communications: A Contemporary Survey. *IEEE Communications Surveys & Tutorials.* 2018, vol. 20, iss. 4, pp. 2889–2922. ISSN 1553-877X. DOI: 10.1109/COMST.2018.2841964.

[2] GUO, H., Y.-C. LIANG, R. LONG, S. XIAO and Q. ZHANG. Resource Allocation for Symbiotic Radio System With Fading Channels. *IEEE Access.* 2019, vol. 7, iss. 1, pp. 34333–34347. ISSN 2169-3536. DOI: 10.1109/ACCESS.2019.2904612.

[3] ZHANG, Q., H. GUO, Y.-C. LIANG and X. YUAN. Constellation Learning-Based

Signal Detection for Ambient Backscatter Communication Systems. *IEEE Journal on Selected Areas in Communications*. 2019, vol. 37, iss. 2, pp. 452–463. ISSN 1558-0008. DOI: 10.1109/JSAC.2018.2872382.

[4] YANG, G., Q. ZHANG and Y.-C. LIANG. Cooperative Ambient Backscatter Communications for Green Internet-of-Things. *IEEE Internet of Things Journal*. 2018, vol. 5, iss. 2, pp. 1116–1130. ISSN 2327-4662. DOI: 10.1109/JIOT.2018.2799848.

[5] ZHAO, W., G. WANG, S. ATAPATTU, C. TEL-LAMBURA and H. GUAN. Outage Analysis of Ambient Backscatter Communication Systems. *IEEE Communications Letters*. 2018, vol. 22, iss. 8, pp. 1736–1739. ISSN 1558-2558. DOI: 10.1109/LCOMM.2018.2842774.

[6] ZHAO, W., G. WANG, R. FAN, L.-S. FAN and S. ATAPATTU. Ambient Backscatter Communication Systems: Capacity and Outage Performance Analysis. *IEEE Access*. 2018, vol. 6, iss. 1, pp. 22695–22704. ISSN 2169-3536. DOI: 10.1109/ACCESS.2018.2828021.

[7] JIA, X. and X. ZHOU. Performance Characterization of Relaying Using Backscatter Devices. *IEEE Open Journal of the Communications Society*. 2020, vol. 1, iss. 1, pp. 819–834. ISSN 2644-125X. DOI: 10.1109/OJCOMS.2020.3003630.

[8] DING, H., D. B. DA COSTA and J. GE. Outage Analysis for Cooperative Ambient Backscatter Systems. *IEEE Wireless Communications Letters*. 2020, vol. 9, iss. 5, pp. 601–605. ISSN 2162-2345. DOI: 10.1109/LWC.2019.2962019.

[9] GUO, H., Y.-C. LIANG, R. LONG and Q. ZHANG. Cooperative Ambient Backscatter System: A Symbiotic Radio Paradigm for Passive IoT. *IEEE Wireless Communications Letters*. 2019, vol. 8, iss. 4, pp. 1191–1194. ISSN 2162-2345. DOI: 10.1109/LWC.2019.2911500.

[10] GONG, S., X. HUANG, J. XU, W. LIU, P. WANG and D. NIYATO. Backscatter Relay Communications Powered by Wireless Energy Beamforming. *IEEE Transactions on Communications*. 2018, vol. 66, iss. 7, pp. 3187–3200. ISSN 1558-0857. DOI: 10.1109/TCOMM.2018.2809613.

[11] ZAWAWI, Z. B., Y. HUANG and B. CLER-CKX. Multiuser Wirelessly Powered Backscatter Communications: Nonlinearity, Waveform Design, and SINR-Energy Tradeoff. *IEEE Transactions on Wireless Communications*. 2019, vol. 18, iss. 1, pp. 241–253. ISSN 1558-2248. DOI: 10.1109/TWC.2018.2879092.

[12] HAN, K. and K. HUANG. Wirelessly Powered Backscatter Communication Networks: Modeling, Coverage, and Capacity. *IEEE Transactions on Wireless Communications*. 2017, vol. 16, iss. 4, pp. 2548–2561. ISSN 1558-2248. DOI: 10.1109/TWC.2017.2665629.

[13] YE Y., L. SHI, R. Q. HU and G. LU. Energy-Efficient Resource Allocation for Wirelessly Powered Backscatter Communications. *IEEE Communications Letters*. 2019, vol. 23, iss. 8, pp. 1418–1422. ISSN 1558-2558. DOI: 10.1109/LCOMM.2019.2920834.

[14] PENG, Y., L. SHANGGUAN, Y. HU, Y. QIAN, X. LIN, X. CHEN, D. FANG and K. JAMIESON. PLoRa: a passive long-range data network from ambient LoRa transmissions. In: *Proceedings of the 2018 Conference of the ACM Special Interest Group on Data Communication (SIGCOMM)*. Budapest: ACM, 2018, pp. 147–160. DOI: 10.1145/3230543.3230567.

[15] WANG, G., F. GAO, R. FAN and C. TEL-LAMBURA. Ambient Backscatter Communication Systems: Detection and Performance Analysis. *IEEE Transactions on Communications*. 2016, vol. 64, iss. 11, pp. 4836–4846. ISSN 1558-0857. DOI: 10.1109/TCOMM.2016.2602341.

[16] QIAN, J., F. GAO, G. WANG, S. JIN and H. ZHU. Noncoherent Detections for Ambient Backscatter System. *IEEE Transactions on Wireless Communications*. 2017, vol. 16, iss. 3, pp. 1412–1422. ISSN 1558-2248. DOI: 10.1109/TWC.2016.2635654.

[17] CHEN, C., G. WANG, Y. WANG and Q. MIAO. Interference Analysis of Ambient Backscatter on Existing Wireless Communication Systems. In: *2017 IEEE 85th Vehicular Technology Conference (VTC Spring)*. Sydney: IEEE, 2017, pp. 1–5. ISBN 978-1-5090-5932-4. DOI: 10.1109/VTC-Spring.2017.8108369.

[18] KIM, S. H. and D. I. KIM. Hybrid Backscatter Communication for Wireless-Powered Heterogeneous Networks. *IEEE Transactions on Wireless Communications*. 2017, vol. 16, iss. 10, pp. 6557–6570. ISSN 1558-2248. DOI: 10.1109/TWC.2017.2725829.

[19] HOANG, D. T., D. NIYATO, P. WANG, D. I. KIM and Z. HAN. Ambient Backscatter: A New Approach to Improve Network Performance for RF-Powered Cognitive Radio Networks. *IEEE Transactions on Communications*. 2017, vol. 65, iss. 9, pp. 3659–3674. ISSN 1558-0857. DOI: 10.1109/TCOMM.2017.2710338.

[20] KANG, X., Y.-C. LIANG and J. YANG. Riding on the Primary: A New Spectrum Sharing Paradigm for Wireless-Powered IoT Devices. *IEEE Transactions on Wireless Communications.* 2018, vol. 17, iss. 9, pp. 6335–6347. ISSN 1558-2248. DOI: 10.1109/TWC.2018.2859389.

[21] AFANA, A., N. ABU-ALI and S. IKKI. On the Joint Impact of Hardware and Channel Imperfections on Cognitive Spatial Modulation MIMO Systems: Cramer–Rao Bound Approach. *IEEE Systems Journal.* 2019, vol. 13, iss. 2, pp. 1250–1261. ISSN 1937-9234. DOI: 10.1109/JSYST.2018.2817598.

[22] SOLANKI, S., P. K. UPADHYAY, D. B. DA COSTA, P. S. BITHAS and A. G. KANATAS. Performance Analysis of Cognitive Relay Networks With RF Hardware Impairments and CEEs in the Presence of Primary Users' Interference. *IEEE Transactions on Cognitive Communications and Networking.* 2018, vol. 4, iss. 2, pp. 406–421. ISSN 2332-7731. DOI: 10.1109/TCCN.2018.2833845.

[23] DING, G., X. GAO, Z. XUE, Y. WU and Q. SHI. Massive MIMO for Distributed Detection With Transceiver Impairments. *IEEE Transactions on Vehicular Technology.* 2018, vol. 67, iss. 1, pp. 604–617. ISSN 1939-9359. DOI: 10.1109/TVT.2017.2747772.

[24] ZHANG, Q., L. ZHANG, Y.-C. LIANG and P.-Y. KAM. Backscatter-NOMA: A Symbiotic System of Cellular and Internet-of-Things Networks. *IEEE Access.* 2019, vol. 7, iss. 1, pp. 20000–20013. ISSN 2169-3536. DOI: 10.1109/ACCESS.2019.2897822.

[25] LE, C.-B. and D.-T. DO. Outage performance of backscatter NOMA relaying systems equipping with multiple antennas. *Electronics Letters.* 2019, vol. 55, iss. 19, pp. 1066–1067. ISSN 1350-911X. DOI: 10.1049/el.2019.1390.

[26] LE, C.-B., D.-T. DO, X. LI, Y.-F. HUANG, H.-C. CHEN and M. VOZNAK. Enabling NOMA in Backscatter Reconfigurable Intelligent Surfaces-Aided Systems. *IEEE Access.* 2021, vol. 9, iss. 1, pp. 33782–33795.

ISSN 2169-3536. DOI: 10.1109/ACCESS.2021.3061429.

[27] GUO, K., B. ZHANG, Y. HUANG and D. GUO. Outage Analysis of Multi-Relay Networks With Hardware Impairments Using SECps Scheduling Scheme in Shadowed-Rician Channel. *IEEE Access.* 2017, vol. 5, iss. 1, pp. 5113–5120. ISSN 2169-3536. DOI: 10.1109/ACCESS.2017.2687479.

[28] DENG, C., M. LIU, X. LI and Y. LIU. Hardware Impairments Aware Full-Duplex NOMA Networks Over Rician Fading Channels. *IEEE Systems Journal.* 2021, vol. 15, iss. 2, pp. 2515–2518. ISSN 1937-9234. DOI: 10.1109/JSYST.2020.2984641.

[29] LI, X., M. ZHAO, M. ZENG, S. MUMTAZ, V. G. MENON, Z. DING and O. A. DOBRE. Hardware Impaired Ambient Backscatter NOMA Systems: Reliability and Security. *IEEE Transactions on Communications.* 2021, vol. 69, iss. 4, pp. 2723–2736. ISSN 1558-0857. DOI: 10.1109/TCOMM.2021.3050503.

About Authors

Minh-Sang VAN NGUYEN was born in Bentre, Vietnam. He is currently pursuing the master's degree in wireless communications. He has worked with the Industrial University of Ho Chi Minh City, Vietnam. His research interests include electronic design, signal processing in wireless communications networks, non-orthogonal multiple access, and physical layer security.

Huu-Phuc DANG (corresponding author) received the B.Sc. degree in electrical electronics engineering from the Ho Chi Minh City University of Technology and Education, Vietnam, in 2004, and the M.Eng. degree in automation control from the Ho Chi Minh City University of Transport, Vietnam, 2012. He is currently pursuing the Ph.D. degree with the Ho Chi Minh City University of Technology and Education, Vietnam. He is also working at Tra Vinh University. His research interest includes signal processing in wireless communications networks and automation control.